

Landau Instability and soliton formations

Shanquan Lan^{1,*} Hong Liu^{2,†} Yu Tian^{3,2,‡} and Hongbao Zhang^{4,5§}

¹ *Department of Physics, Lingnan Normal University, Zhanjiang 524048, China*

² *Center for Theoretical Physics, Massachusetts Institute of Technology, Cambridge, MA 02139, USA*

³ *School of Physics, University of Chinese Academy Sciences, Beijing 100049, China*

⁴ *Department of Physics, Beijing Normal University, Beijing 100875, China*

⁵ *Theoretische Natuurkunde, Vrije Universiteit Brussel,*

and The International Solvay Institutes, Pleinlaan 2, B-1050 Brussels, Belgium

Consider at a finite temperature T a superfluid moving with a velocity v relative to the thermal bath or its normal component. From Landau's argument there exists a critical $v_c(T)$ beyond which excitations can be spontaneously generated and the system becomes unstable. Identifying the final state induced by such an instability has been an outstanding open question. Using holographic duality we perform dynamical simulations of evolutions from initial unstable states, and find that the system settles to a homogenous superfluid state with a final velocity below the critical velocity. The dynamical evolution process appears to be highly chaotic, exhibiting transient turbulence. Nevertheless we are able to identify from the simulations a universal physical mechanism for the reduction of superfluid velocity, in terms of spontaneous nucleation of solitons. We also derive a simple analytic formula which relates the final velocity to the number of solitons nucleated during the evolution.

Introduction.—At zero temperature, a superfluid flows in a pipe without friction until its velocity v exceeds the Landau critical velocity v_c [1]. Beyond v_c , excitations can be spontaneously generated, and lead to dissipation. If the cross section of the pipe is large, excitations are created near the boundary, but the superfluid bulk can still flow with $v > v_c$ sufficiently far away from the boundary. (In an infinite space, a superfluid can flow at any velocity without creating excitations due to boost invariance.)

Now consider a finite temperature T and a superfluid moving with a velocity v relative to the thermal bath or its normal component. From Landau's argument there should exist a critical $v_c(T)$ beyond which excitations can be spontaneously generated. But now since excitations are created everywhere, the system should develop a genuine instability. What is the final state resulting from the instability? Will superfluidity disappear or will the system become inhomogeneous?

In this paper, from studying holographic superfluids, we show that a superfluid with an initial velocity $v_i > v_c(T)$ transitions to a homogeneous superfluid state with a final velocity $v_f < v_c(T)$ via a remarkably simple and elegant mechanism: the superfluid velocity is reduced by spontaneously nucleating solitons. The dynamical evolution process from the initial unstable supercritical state to the final state appears to be highly chaotic, exhibiting transient turbulence. But the final velocity can be determined in a simple way from the number of solitons nucleated during the transition process.

This physical mechanism is universal, not depending on specific details of a system. It can in principle be

directly tested in cold atomic systems and should have wide applications.

Simulating full dynamical evolution of a superfluid at a finite temperature is a challenging problem, for which there is no satisfactory conventional method. An often-used approach, the dissipative Gross-Pitaevskii equation—where one introduces dissipative effects by hand—is rather crude and requires significant modeling. This motivates us to turn to holographic duality, which equates certain strongly correlated systems of quantum matter to classical gravitational systems in a curved spacetime with one extra spatial dimension. In this framework, a superfluid at a finite temperature is described by a hairy black hole where finite temperature dissipative effects are incorporated from first principle: once the microscopical theory is fixed, all aspects of the superfluid phase are determined without any phenomenological modeling. Furthermore, the gravity description is particularly powerful for simulating real-time dynamical evolution of far-from-equilibrium quantum systems by converting such problems to solvable problems of numerical relativity (see [2] for recent reviews).

Holographic setup, dispersion relations, and linear instability of superflow.— We first review the results of [3], which shows that there exists a critical velocity beyond which a holographic superfluid becomes unstable¹. As such, we will consider a $(2+1)$ -dimensional superfluid, which can be described by an Abelian-Higgs model [4, 5]

$$\mathcal{L} = -\frac{1}{4}F_{ab}F^{ab} - |D\Psi|^2 - m^2|\Psi|^2 \quad (1)$$

* lansq@lingnan.edu.cn

† hong_liu@mit.edu

‡ ytian@ucas.ac.cn

§ hzhang@vub.ac.be

¹ Please refer to the supplementary material for the details about our numerics, which is different from that used in [3].

in a (3 + 1)-dimensional AdS black hole spacetime

$$ds^2 = \frac{L^2}{z^2}(-f(z)dt^2 - 2dt dz + d\mathbf{x}^2). \quad (2)$$

Here $\mathbf{x} = (x, y)$, L is the AdS radius, and $f(z) = 1 - (\frac{z}{z_h})^3$. $z = z_h$ is the black hole horizon and $z = 0$ is the AdS boundary. The AdS black hole has a Hawking temperature $T = \frac{3}{4\pi z_h}$, which gives the temperature of the dual boundary system. Ψ is a complex scalar field dual to a boundary order parameter O , and $D_a = \nabla_a - iA_a$ where ∇ is the covariant derivative associated with the metric, and the $U(1)$ gauge field A_a is dual to a conserved global $U(1)$ current j^μ under which O is charged. The chemical potential μ for the global $U(1)$ symmetry is specified by the boundary value of A_t , i.e. $\mu = A_t(z = 0)$, and the corresponding charge density ρ is given by $\rho = -\partial_z A_t(z = 0)$ in the axial gauge $A_z = 0$. Throughout the paper we will keep the total charge of the system fixed.

The system enters a superfluid phase below some critical temperature T_c when the order parameter O develops a nonzero expectation value, which in the gravity description corresponds to the condensation of Ψ . The superfluid dynamics is governed by the equations

$$D_a D^a \Psi - m^2 \Psi = 0, \quad \nabla_a F^{ab} = i(\bar{\Psi} D^b \Psi - \Psi \bar{D}^b \bar{\Psi}). \quad (3)$$

For definiteness we take $m^2 = -\frac{2}{L^2}$, for which there are two possible boundary conditions for Ψ , leading to two different types of superfluids with O having dimensions 2 and 1, respectively. Below we focus on the one corresponding to O having dimension 2. We will denote $\psi = \langle O \rangle$.

Flow of the superfluid component can be generated by turning on a source \mathbf{a} for the spatial components of $U(1)$ current \mathbf{j} . Here and below bold-face letters always denote vectors in boundary spatial directions. With

$$\begin{aligned} \mathcal{J} &= \frac{i}{2}[\psi(\partial + i\mathbf{a})\bar{\psi} - \bar{\psi}(\partial - i\mathbf{a})\psi], \\ \mathcal{J}_t &= \frac{i}{2}[\psi(\partial_t + i\mu)\bar{\psi} - \bar{\psi}(\partial_t - i\mu)\psi], \end{aligned} \quad (4)$$

the superfluid velocity can be written as

$$\mathbf{v} = \frac{\mathcal{J}}{\mathcal{J}_t} = -\frac{\mathbf{a} - \partial\theta}{\mu - \partial_t\theta}, \quad (5)$$

where θ is the phase of $\psi = |\psi|e^{i\theta}$. In the gravity description \mathbf{a} can be identified as the boundary value of the bulk gauge field A_a in (x, y) directions. We will take \mathbf{a} to be in the x -direction, so is the induced superflow.

With the boundary condition fixed, the superflow solution can be obtained by solving the equations of motion (3). In FIG. 1, we show how the magnitude of the superfluid condensate depends on the superfluid velocity. Notice that the magnitude decreases with the velocity, with the condensate disappearing beyond a certain critical value v_{c1} . The system in fact already becomes

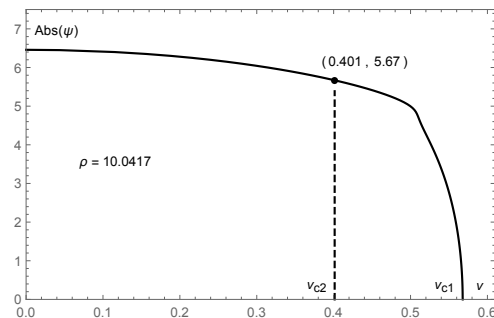


FIG. 1. The superfluid condensate as a function of the superfluid velocity at $\frac{T}{T_c} = 0.637$.

unstable at a value $v_{c2} < v_{c1}$, which can be seen from a linear response analysis. Due to translational symmetries along the boundary directions, it is convenient to decompose small perturbations around a superflow solution in terms of Fourier modes $e^{-i\omega t + i\mathbf{k}\cdot\mathbf{x}}$. Solving linearized equations of motion (3) we find a discrete spectrum of quasinormal modes $\omega(\mathbf{k})$, which are complex due to dissipations into the normal component. The lowest mode is the sound mode and for $v = 0$ has the dispersion relation $\omega(\mathbf{k}) = c_s|\mathbf{k}| - i\gamma|\mathbf{k}|^2$ (for small $|\mathbf{k}|$), where c_s is the sound speed and γ characterizes its attenuation. For example, for $T/T_c = 0.637$ we have $c_s = 0.63$. With a nonzero v , the system is no longer isotropic, accordingly c_s and γ become direction-dependent. The maximal and minimal values of c_s are achieved in directions parallel (with $k_x > 0, k_y = 0$) and anti-parallel (with $k_x < 0, k_y = 0$) with the superflow. We will denote them respectively as $c_s^\pm(v)$, and the corresponding values for γ will be denoted as γ^\pm .

In FIG. 2 we plot the dispersion relations with $k_y = 0$ for various values of v . We notice that as v increases beyond a certain value $v_{c2} = 0.401$, c_s^- becomes negative, and thus the excitation energy becomes negative. This is consistent with the expectation of Landau's argument. Furthermore, beyond the same value of v_{c2} , γ^- changes sign and $\text{Im}\omega(\mathbf{k})$ becomes positive for sufficiently small $|k_x|$, signaling that the system becomes unstable. See FIG. 3 for the phase diagram of the system.

Full nonlinear simulations, soliton formations and final state of unstable superflow.— We now examine the final state of the instability using full nonlinear simulation. We use units in which temperature is $T = \frac{3}{4\pi}$ and work in a $R \times R$ periodic box with $R = 30$, which is large enough such that the boundary effect is negligible for the physics we are concerned with here. The system is evolved with an initial configuration of the form $\Psi_0(z, \mathbf{x}) = \Psi_b(z)e^{i\chi(\mathbf{x})}$ where $\Psi_b(z)$ is the background solution for the unstable superflow, and

$$\chi(\mathbf{x}) = c \text{Re} \sum_{\mathbf{k}} \xi(\mathbf{k}) e^{i\mathbf{k}\cdot\mathbf{x}} \quad (6)$$

with c a small real constant and $\xi(\mathbf{k})$ a set of $\mathcal{O}(1)$ ran-

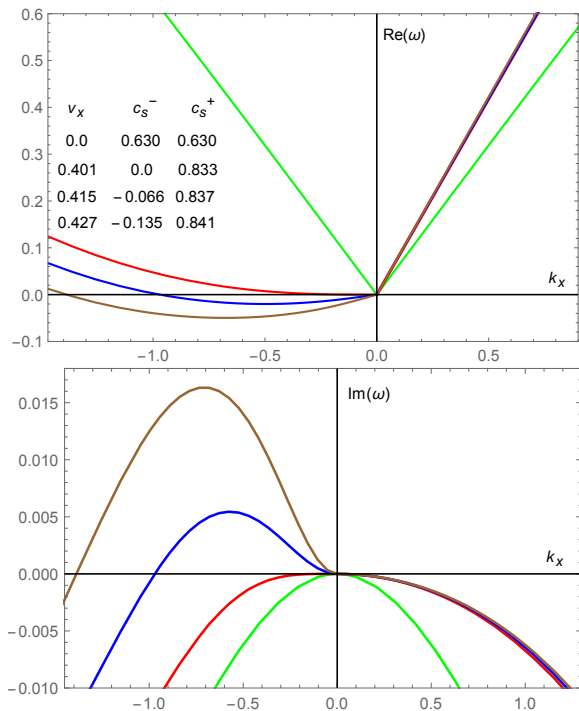


FIG. 2. The dispersion relation of sound modes for $k_y = 0$ at $\frac{T}{T_c} = 0.637$, where the green, red, blue, and brown lines are for velocity $v = 0, 0.401, 0.415, 0.427$. The corresponding values of c_s^\pm are also listed. The onset of instability is signaled by the red line, where $c_s^- = 0$ and $\gamma^- = 0$.

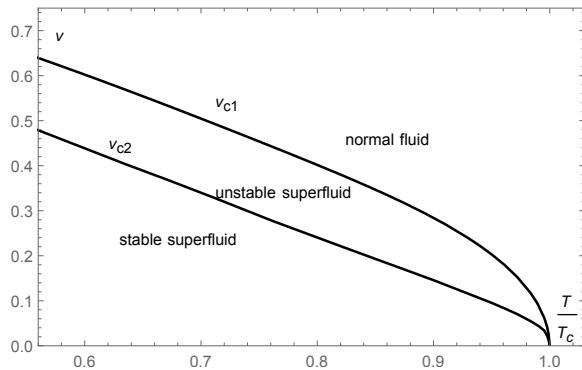


FIG. 3. The phase diagram for superflow, where the unstable superfluid and stable superfluid are separated by v_{c2} .

dom complex coefficients. For comparisons we also consider one-dimensional (1D) simulations by freezing the dynamics along the y direction.

In FIG. 4 we plot the time evolution of the average superfluid velocity along x direction for a typical initial configuration in both 1D and 2D, which shows that after some time, \bar{v}_x in both cases decreases and settles eventually down to a value less than the critical velocity v_{c2} . Notice while the 1D curve exhibits a step-function-like drop, the 2D curve can be fitted by two segments of lin-

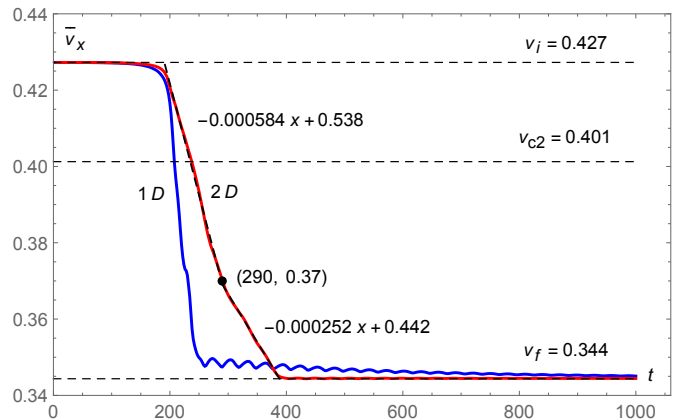


FIG. 4. The averaged superfluid velocity as a function of time, where the blue and red lines denote the 1D and 2D superflow respectively at $\frac{T}{T_c} = 0.637$ with the intermediate horizontal dashed line indicating the corresponding critical velocity. For comparison, we specifically choose simulations such that the 1D and 2D cases have the same final velocity. The velocity decrease in the 2D case can be fitted by two linear segments, with their respective slopes indicated in the plot.

ear decrease. The simulations also show that while the system is highly inhomogeneous and chaotic in intermediate times, $|\psi|$ becomes homogeneous in the final state.

To identify the physical mechanism for the reduction of the superfluid velocity and the physical nature of the final state, we will explore the time evolution from two other perspectives. We first consider the 1D case which serves as a simpler example to illustrate the key points. In FIG. 5 we plot the behavior of $|\psi(x)|$ in 1D case at various times. We have specifically included the plots at $t = 206, 218, 236$, around when a dark soliton (where $|\psi|$ reaches 0) is formed briefly. Notice the time range of soliton formations precisely coincides with that of the sharp drop in \bar{v}_x in FIG. 4, which strongly hints that the physical mechanism for transitioning to the final stable state should have to do with soliton formations.

To understand this point more precisely, in FIG. 6 we plot snapshots of the condensate $\psi(t, x)$ on the complex ψ -plane, with each plotted point corresponding to the value of $\psi(t, x)$ for some given t and x . Since we consider a periodic box, at a given time all the points form a closed loop in the complex ψ -plane. Such plots have the advantage of showing the variations of both the magnitude and the phase of the condensate over space and time. For example, for a uniform condensate, the whole curve collapses to a single point on the complex ψ -plane, whose distance from the origin gives $|\psi|$ and polar angle gives the phase of ψ . At very early times, when the condensate is approximately uniform we see that the whole loop is indeed localized in a small region of the ψ -plane. As the system evolves, the curve quickly expands in a highly irregular manner, reflecting rapid and chaotic growth of inhomogeneity in both the magnitude and phase.

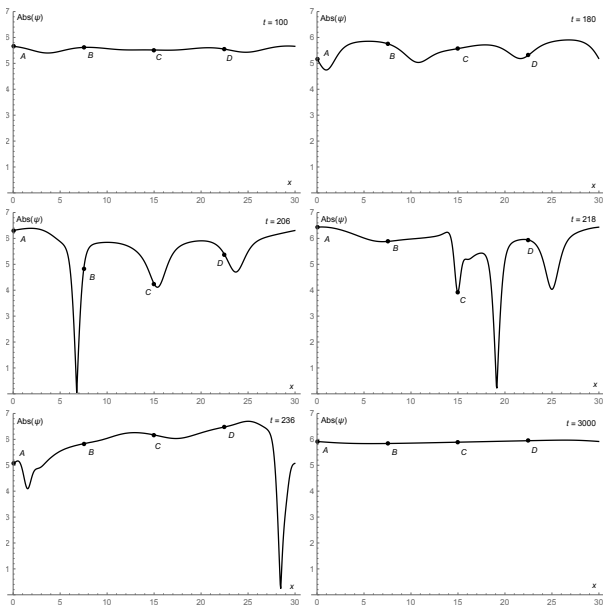


FIG. 5. Plots of $|\psi(x)|$ at different times for the 1D curve of FIG. 4. We start with an initial unstable superflow state with small inhomogeneous disturbances. The inhomogeneity quickly grows as time evolves, but eventually settles to a final state with uniform $|\psi(x)|$. There is a dark soliton briefly appearing around $t = 206, 218, 236$, respectively.

The soliton formations in FIG. 5 at $t = 206, 218, 236$ are reflected in FIG. 6 as the loop passing through the origin of the complex ψ -plane. Now the implication of a soliton formation can be readily understood: it results in a nontrivial winding between the phase θ and the physical space. More explicitly, before $t = 206$ we have $\theta(R) - \theta(0) = 0$, but after that we have $\theta(R) - \theta(0) = -2\pi$. Similarly, soliton formations at $t = 218$ and $t = 236$ generate two additional windings. As indicated in the last plot ($t = 3000$) of FIG. 6, both the magnitude $|\psi|$ and the variation of the phase of the final state are expected to be homogeneous along x direction with $\theta(R) - \theta(0) = -3 \times 2\pi$.

Now the connection between soliton formation and the drop in velocity is clear. From Eq. (5), the initial velocity is $v_i = -a_x/\mu_i$, where μ_i is the initial chemical potential. The final velocity is given by $v_f = -\frac{1}{\mu_f}(a_x + \frac{2\pi n}{R})$ where n is the number of dark solitons formed during the evolution process and μ_f is the final chemical potential. We thus find a simple elegant relation between the initial and final velocities

$$v_f = \frac{1}{\mu_f} \left(\mu_i v_i - \frac{2\pi n}{R} \right). \quad (7)$$

For the 1D example of FIG. 4, we have $\mu_i = 6.553$, $\mu_f = 6.306$, and $n = 3$. With those values we see that the numerical values of v_i and v_f given in FIG. 4, obtained from full nonlinear simulations, satisfy the above equation very well.

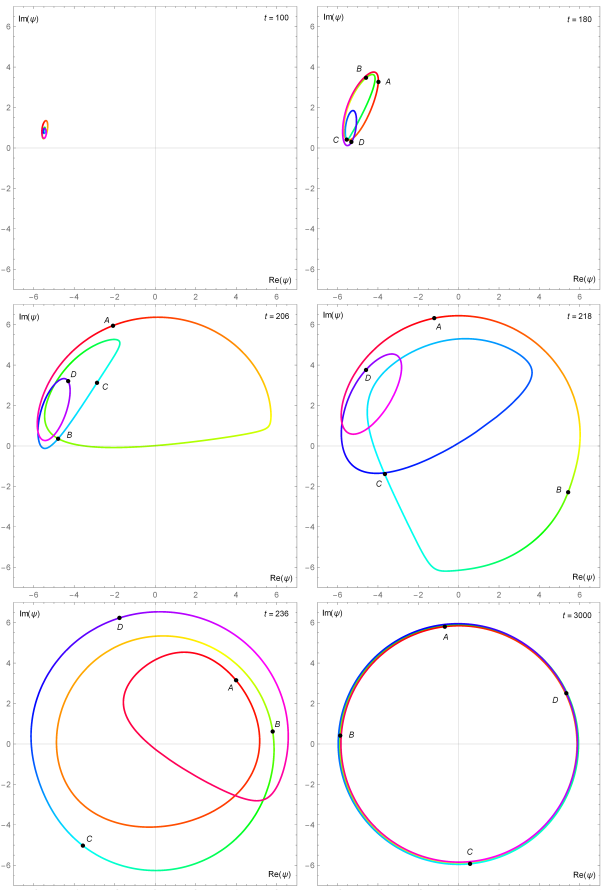


FIG. 6. The snapshots of superfluid condensate for the 1D curve of FIG. 4. Points A, B, C, D denote the spatial locations $x = 0, R/4, R/2, 3R/4$, respectively. The corresponding points are also highlighted in FIG. 5.

We note, however, the number of solitons formed during the process and thus the final velocity depend on the initial disturbance (6). We find that if we keep the “strength” c fixed while increasing the number of initial modes, more solitons are generated and thus the smaller the final velocity. When we keep the number of initial modes fixed, but vary c , the number of solitons does not change with a pretty wide range of c . When we keep everything else fixed, but increase the size R of the box, the number of solitons formed increases linearly with R , and the final velocity does not change.

The 2D story works similarly to that of 1D, with formation of dark solitons now replaced by nucleation of vortex-antivortex pairs. In FIG. 7, we give the density plot of the condensate at various times. For example, two vortex-antivortex pairs are formed around the same time between $t = 200$ and $t = 205$. When they are formed, vortex and antivortex move in opposite directions along the y -axis (i.e. perpendicular to the direction of the superflow) with a constant velocity $u_y \approx 0.13$. This may be understood as a result of opposite Magnus force they

each experience, and the balance between the Magnus force and friction. Since the box is periodic, the vortex and antivortex in a pair will meet again and annihilate after $t = \frac{R}{2u_y}$. They may also annihilate with vortices from other pairs if they happen to meet. All vortices also move along with the superfluid in x -direction.

The effect of vortex formations on superfluid flow velocity is as follows: when a vortex (or anti-vortex) passes a horizontal line $y = y_0$, the winding of the condensate in x -direction at y_0 reduces by 1.² Thus the superflow velocities in the horizontal strip between the vortex and anti-vortex are reduced, as indicated in FIG. 8. When the vortex and anti-vortex meet again and annihilate, the x -winding for the whole box will have reduced by 1. Suppose that a vortex pair is formed at t_0 , when the velocity of superflow is v_0 , and that these are the only vortices in the system, then for $0 < \delta t = t - t_0 < \frac{R}{2u_y}$, the average velocity is given by $\bar{v}(t) = \frac{1}{R} \left(v_0(R - 2u_y\delta t) + (v_0 - \frac{2\pi}{\mu R})2u_y\delta t \right) = v_0 - \frac{4\pi u_y(t-t_0)}{\mu R^2}$. We see that the velocity decreases linearly with t with a slope $-\frac{4\pi u_y}{\mu R^2}$. The pair annihilates at $t = t_0 + \frac{R}{2u_y}$ after which the average velocity remains constant until the next vortex formation. When there are multiple vortex pairs in the system at a given time, we simply add their effects. In general when there are n pairs of vortices in the system, we have

$$\text{slope} = -\frac{4\pi n u_y}{\mu R^2}. \quad (8)$$

In FIG. 7, before $t = 200$, there is no vortex. During the time period from $t = 200$ to $t = 290$ there are on average 2 pairs of vortices at a given time (sometimes 3 pairs). From $t = 290$ to $t = 400$, there are on average 1 pair of vortices at a time. After $t = 400$ there is no vortex left. We see in FIG. 4, the 2D plot exhibits indeed two linear regimes in the stated time ranges, with slopes as indicated in the figure. Their values agree reasonably well with the estimates using (8), which gives -5.6×10^{-4} and -2.8×10^{-4} respectively for $n = 2$ and $n = 1$ (using $\mu \approx 6.5$).

To summarize, in 1D, since solitons are co-dimension one, they lead to sudden drop in the average velocity, while in 2D vortex formations lead to piece-wise linear decrease. Also notice in FIG. 4 that the 1D curve exhibits a long tail approaching the final value, which is not present for 2D. The tail can be explained as follows: the solitons in 1D decay through a process similar to self-acceleration [6], which eventually leads to sound waves that mostly propagate in the direction of the superflow and it takes a long time for the sound waves to dissipate. We have indeed checked quantitatively that both

² If we make plots like FIG. 6 for 2D by restricting to a single value $y = y_0$, then when a vortex passes, the loop passes the origin of the ψ -plane and a winding is generated. The sign of the winding change does not depend on whether it is a vortex or anti-vortex.

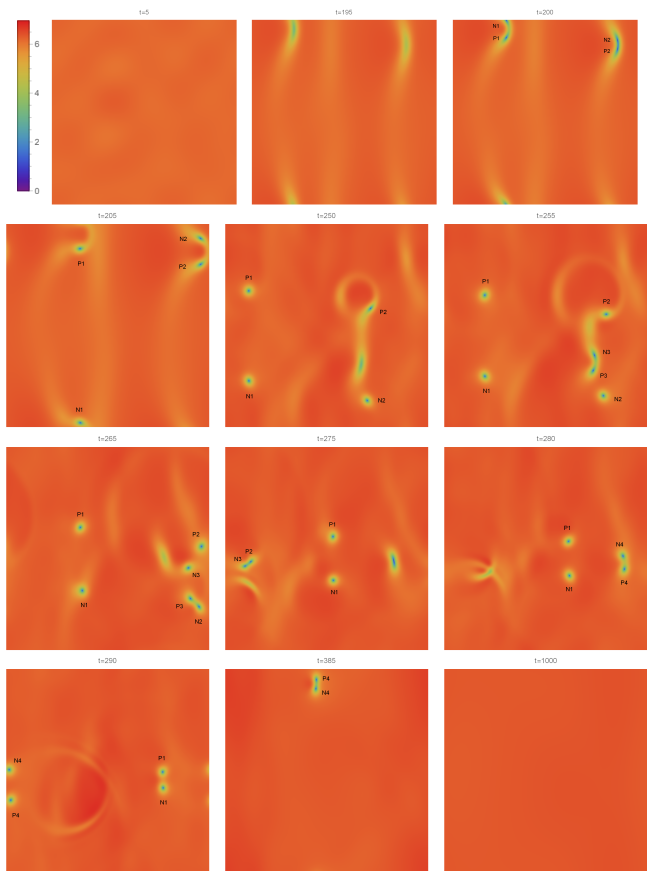


FIG. 7. The snapshots for the density plot of 2D superfluid condensate for the 2D curve of FIG. 4. Vortices and anti-vortices are labeled by P and N , respectively.



FIG. 8. The cartoon for the decrease of the superfluid velocity by the departure of a formed vortex pair from each other.

the decay rate and oscillation frequency of the tail of the 1D curve can be well explained in terms of the dispersion relations of sound waves of the final state. For 2D, since vortices are co-dimension two, the sound waves they generated occupy a small fraction of total volume of the system and thus have much less significant effects.

Conclusion and discussion.—To conclude, from full nonlinear simulations, we have found that an unstable superflow evolves into a homogeneous state with a velocity less than the critical velocity. Furthermore, we have identified generation of winding numbers from dark soli-

ton/vortex formations as the underlying physical mechanism. The real-time evolution exhibits transient turbulent behavior. It is natural to expect that if we keep driving the system so that it remains above the critical velocity, we should find a steady turbulent state. Indeed this is the case and will be reported elsewhere.

We expect that the physical mechanism uncovered here, i.e. the system reduces velocity by nucleating solitons, should have wide applications. Here we mention two examples. In [7], a supersonically expanding ring-shaped Bose-Einstein condensate was studied and production of solitons and vortices was observed. The mechanism of our paper provides a natural explanation for the physics behind these soliton productions. In [8, 9], rotating superfluids were studied and vortex generation was observed near the edge of the superfluid, but not in the interior. Again our mechanism provides a simple explanation: the edge of the rotating superfluid has the largest linear velocity and when it exceeds the critical velocity, vortices are then formed near the edge to reduce the velocity.

Acknowledgements.—This work is partially supported by NSFC with Grant No. 11675015, 11775022, 11847001, 11875095, 11975235, 12005008, and 12075026. S.L. is supported by Yanling Young Teacher Program of Lingnan Normal University. H.L. is supported by the Office of High Energy Physics of U.S. Department of Energy under grant Contract Number DE-SC0012567. Y.T. is supported by the Strategic Priority Research Program of the Chinese Academy of Sciences with Grant No.XDB23030000. H.Z. is supported in part by FWO-Vlaanderen through the project G006918N, and by the Vrije Universiteit Brussel through the Strategic Research Program “High-Energy Physics”. He is also an individual FWO Fellow supported by 12G3518N.

SUPPLEMENTAL MATERIAL

Below, we describe the involved numerics in detail for those who are interested.

For convenience in our numerical calculations, we will take $L = 1$ as our unit, and fix $z_h = 1$. Then the relevant results can be obtained by the scaling symmetry of the system. In addition, we define a new function $\Phi = \frac{\Psi}{z}$ and work with the axial gauge $A_z = 0$, in which the bulk equations of motion can be written explicitly as

$$\partial_t \partial_z \Phi = i A_t \partial_z \Phi + \frac{1}{2} [i \partial_z A_t \Phi + f \partial_z^2 \Phi + f' \partial_z \Phi + (\partial - i A)^2 \Phi - z \Phi], \quad (9)$$

$$\partial_z (\partial_z A_t - \partial \cdot \mathbf{A}) = i (\bar{\Phi} \partial_z \Phi - \Phi \partial_z \bar{\Phi}), \quad (10)$$

$$\partial_t \partial_z \mathbf{A} = \frac{1}{2} [\partial_z (\partial A_t + f \partial_z \mathbf{A}) + (\partial^2 \mathbf{A} - \partial \partial \cdot \mathbf{A}) - i (\bar{\Phi} \partial \Phi - \Phi \partial \bar{\Phi})] - \mathbf{A} \bar{\Phi} \Phi, \quad (11)$$

$$\partial_t \partial_z A_t = \partial^2 A_t + f \partial_z \partial \cdot \mathbf{A} - \partial_t \partial \cdot \mathbf{A} - 2 A_t \bar{\Phi} \Phi + i f (\bar{\Phi} \partial_z \Phi - \Phi \partial_z \bar{\Phi}) - i (\bar{\Phi} \partial_t \Phi - \Phi \partial_t \bar{\Phi}). \quad (12)$$

As a result, the asymptotic solution of A and Φ near the AdS boundary can be expanded as

$$A_\mu = a_\mu + b_\mu z + o(z), \quad \Phi = \phi + \psi z + o(z). \quad (13)$$

According to the holographic dictionary, the expectation value of j and O can be obtained explicitly by the variation of renormalized bulk on-shell action with respect to the source as

$$\langle j^\mu \rangle = \frac{\delta S_{ren}}{\delta a_\mu} = \lim_{z \rightarrow 0} \sqrt{-g} F^{z\mu}, \quad (14)$$

$$\begin{aligned} \langle O \rangle &= \frac{\delta S_{ren}}{\delta \phi} = - \lim_{z \rightarrow 0} z \sqrt{-h} (n_a D^a \Psi + \Psi) \\ &= \psi - \dot{\phi} + i a_t \phi, \end{aligned} \quad (15)$$

where the dot denotes the time derivative, and the renormalized action is given by

$$S_{ren} = \int_{\mathcal{M}} \sqrt{-g} \mathcal{L} - \int_{\mathcal{B}} \sqrt{-h} |\Psi|^2 \quad (16)$$

with the counter term added to make the original action finite.

For our purpose, we set $a_t = const, a_x = const, a_y = 0, \phi = 0$, thus Eq.(12) evaluated at the AdS boundary reduces to

$$\partial_t \rho = -\partial_z \partial \cdot \mathbf{A}|_{z=0}, \quad (17)$$

which is essentially the conservation law of charge current.

With the above boundary conditions and the periodic boundary condition along the \mathbf{x} direction, the full nonlinear simulations are performed by employing the pseudo-spectral method with 28 Chebyshev modes in the z direction and 121 Fourier modes in the \mathbf{x} direction, as well as the fourth order Runge-Kutta method in time direction with the time step $\Delta t = 0.05$.

On the other hand, the laminar superflow solutions can be obtained by solving the equations of motion with the non-vanishing bulk fields dependent only on z , which are simplified as

$$f\partial_z\theta + A_t = 0, \quad (18)$$

$$2\partial_z\theta\phi^2 + \partial_z^2 A_t = 0, \quad (19)$$

$$f\partial_z^2 A_x + f'\partial_z A_x - 2A_x\phi^2 = 0, \quad (20)$$

$$f\partial_z^2\phi + f'\partial_z\phi - (z + A_x^2 + 2A_t\partial_z\theta + f(\partial_z\theta)^2)\phi = 0, \quad (21)$$

where we have rewritten Φ as $\phi(z)e^{i\theta(z)}$, and specified the x direction as the superflow direction.

The onset of Landau instability of such superflow solutions can be analyzed by the linear response theory. To be more specific, we first decompose the background complex scalar function into its real and imaginary parts as $\Phi(z) = \phi(z)e^{i\theta(z)} = \Phi_r(z) + i\Phi_i(z)$, and then write all the perturbation functions in terms of the form $\delta(z)e^{-i\omega t + ik\cos\alpha x + ik\sin\alpha y}$. As a result, the lin-

earized perturbation equations can be expressed as

$$\begin{aligned} 0 = & (z + k^2 + A_x^2 + (3z^2 - 2i\omega)\partial_z - f\partial_z^2)\delta\Phi_r \\ & + (\partial_z A_t - 2ik\cos\alpha A_x + 2A_t\partial_z)\delta\Phi_i \\ & + (2\partial_z\Phi_i + \Phi_i\partial_z)\delta A_t \\ & + (2A_x\Phi_r - ik\cos\alpha\Phi_i)\delta A_x \\ & - ik\sin\alpha\Phi_i\delta A_y, \end{aligned} \quad (22)$$

$$\begin{aligned} 0 = & (-\partial_z A_t + 2ik\cos\alpha A_x - 2A_t\partial_z)\delta\Phi_r \\ & + (z + k^2 + A_x^2 + (3z^2 - 2i\omega)\partial_z - f\partial_z^2)\delta\Phi_i \\ & + (-2\partial_z\Phi_r - \Phi_r\partial_z)\delta A_t \\ & + (2A_x\Phi_i + ik\cos\alpha\Phi_r)\delta A_x \\ & + ik\sin\alpha\Phi_r\delta A_y, \end{aligned} \quad (23)$$

$$\begin{aligned} 0 = & (-2i\omega\Phi_i + 4A_t\Phi_r)\delta\Phi_r \\ & + (2i\omega\Phi_r + 4A_t\Phi_i)\delta\Phi_i \\ & + (k^2 + 2(\Phi_r^2 + \Phi_i^2) - i\omega\partial_z - f\partial_z^2)\delta A_t \\ & + \omega k\sin\alpha\delta A_x \\ & + \omega k\cos\alpha\delta A_y, \end{aligned} \quad (24)$$

$$\begin{aligned} 0 = & (4A_x\Phi_r + 2ik\sin\alpha\Phi_i)\delta\Phi_r \\ & + (4A_x\Phi_i - 2ik\sin\alpha\Phi_r)\delta\Phi_i - ik\sin\alpha\partial_z\delta A_t \\ & + (2(\Phi_r^2 + \Phi_i^2) + (k\cos\alpha)^2 + (3z^2 - 2i\omega)\partial_z - f\partial_z^2)\delta A_x \\ & - k^2\sin\alpha\cos\alpha\delta A_y, \end{aligned} \quad (25)$$

$$\begin{aligned} 0 = & 2ik\cos\alpha\Phi_i\delta\Phi_r - 2ik\cos\alpha\Phi_r\delta\Phi_i \\ & - ik\cos\alpha\partial_z\delta A_t - k^2\sin\alpha\cos\alpha\delta A_x \\ & + (2(\Phi_r^2 + \Phi_i^2) + (k\sin\alpha)^2 + (3z^2 - 2i\omega)\partial_z - f\partial_z^2)\delta A_y. \end{aligned} \quad (26)$$

The corresponding quasinormal modes are extracted by solving the above generalized eigenvalue problem on top of the background superflow solution.

-
- [1] E. M. Lifshitz and L. P. Pitaevskii, *Statistical Physics II*, (Pergamon Press, Oxford, 1980).
[2] H. Liu, and J. Sonner, arXiv:1810.11424[hep-th].
[3] I. Amado, D. Areal, A. Jimenez-Alba, K. Landsteiner, L. Melgar and I. Salazar, *JHEP* **02**, 063(2014).
[4] S. A. Hartnoll, C. P. Herzog, and G. T. Horowitz, *Phys. Rev. Lett.* **101**, 031601(2008).
[5] S. A. Hartnoll, C. P. Herzog, and G. T. Horowitz, *JHEP*

- 12**, 015(2008).
[6] M. Guo, E. Keski-Vakkuri, H. Liu, Y. Tian and H. Zhang, *Phys. Rev. Lett.* **124**, 031601(2020).
[7] S. Eckel, A. Kumar, T. Jacobson, I. B. Spielman and G. K. Campbell, *Phys. Rev. X* **8**, 021021(2018).
[8] X. Li, Y. Tian and H. Zhang, *JHEP* **02**, 104(2020).
[9] C. Xia, H. Zeng, H. Zhang, Z. Nie, Y. Tian and X. Li, *Phys. Rev. D* **100**, 061901(2019)